

RESEARCH ARTICLE

Monitoring apoptosis in intact cells by high-resolution magic angle spinning ^1H NMR spectroscopyMarta Wylot¹ | David T.E. Whittaker² | Stephen A.C. Wren³ | John H. Bothwell⁴ | Leslie Hughes³ | Julian L. Griffin^{1,5} ¹Department of Biochemistry, University of Cambridge, Cambridge, UK²Early Chemical Development, Pharmaceutical Sciences, R&D, AstraZeneca, Macclesfield, UK³New Modalities & Parenteral Development, Pharmaceutical Technology & Development, Operations, AstraZeneca, Macclesfield, UK⁴Department of Biosciences, University of Durham, Durham, UK⁵Section of Biomolecular Medicine, Department of Metabolism, Digestion and Reproduction, Imperial College London, London, UK**Correspondence**Julian L. Griffin, Sir Alexander Fleming Building, South Kensington Campus, Imperial College London, London SW7 2AZ, UK.
Email: julian.griffin@imperial.ac.uk**Funding information**

Engineering and Physical Sciences Research Council ICASE studentship in conjunction with Astra Zeneca, Grant/Award Number: Studentship Reference 1789837; Medical Research Council, Grant/Award Number: MR/P011705/1

Apoptosis maintains an equilibrium between cell proliferation and cell death. Many diseases, including cancer, develop because of defects in apoptosis. A known metabolic marker of apoptosis is a notable increase in ^1H NMR-observable resonances associated with lipids stored in lipid droplets. However, standard one-dimensional NMR experiments allow the quantification of lipid concentration only, without providing information about physical characteristics such as the size of lipid droplets, viscosity of the cytosol, or cytoskeletal rigidity. This additional information can improve monitoring of apoptosis-based cancer treatments in intact cells and provide us with mechanistic insight into why these changes occur.

In this paper, we use high-resolution magic angle spinning (HRMAS) ^1H NMR spectroscopy to monitor lipid concentrations and apparent diffusion coefficients of mobile lipid in intact cells treated with the apoptotic agents cisplatin or etoposide. We also use solution-state NMR spectroscopy to study changes in lipid profiles of organic solvent cell extracts. Both NMR techniques show an increase in the concentration of lipids but the relative changes are 10 times larger by HRMAS ^1H NMR spectroscopy. Moreover, the apparent diffusion rates of lipids in apoptotic cells measured by HRMAS ^1H NMR spectroscopy decrease significantly as compared with control cells. Slower diffusion rates of mobile lipids in apoptotic cells correlate well with the formation of larger lipid droplets as observed by microscopy. We also compared the mean lipid droplet displacement values calculated from the two methods. Both methods showed shorter displacements of lipid droplets in apoptotic cells. Our results demonstrate that the NMR-based diffusion experiments on intact cells discriminate between control and apoptotic cells. Apparent diffusion measurements in conjunction with ^1H NMR spectroscopy-derived lipid signals provide a novel means of following apoptosis in intact cells. This method could have potential application in enhancing drug discovery by monitoring drug treatments in vitro, particularly for agents that cause partitioning of lipids such as apoptosis.

Abbreviations: ANOVA, analysis of variance; BODIPY, boron dipyrromethene; COSY, correlation spectroscopy; D , diffusion constant [$\text{m}^2\cdot\text{s}^{-1}$]; DMEM, Dulbecco's modified Eagle's medium; DMSO, dimethyl sulfoxide; DOSY, diffusion-ordered spectroscopy; HRMAS NMR, high-resolution magic angle spinning NMR; k , Boltzmann's constant [$\text{m}^2\cdot\text{kg}\cdot\text{s}^{-2}\cdot\text{K}^{-1}$]; LD, lipid droplet; MRS, magnetic resonance spectroscopy; PBS, phosphate buffered saline; PC, principal component; PCA, principal component analysis; r , radius of diffusing particle [m]; SEM, standard error of the mean; T , temperature [K]; TMS, tetramethylsilane; TSP, trimethylsilylpropanoic acid; ν , viscosity [$\text{kg}\cdot\text{m}^{-1}\cdot\text{s}^{-1}$]; W4M, Workflow4Metabolomics.

This is an open access article under the terms of the Creative Commons Attribution License, which permits use, distribution and reproduction in any medium, provided the original work is properly cited.

© 2021 The Authors. *NMR in Biomedicine* published by John Wiley & Sons Ltd.

KEYWORDS

applications, biophysical mechanisms of MR diffusion, cancer, cancer therapy responses, cells and biofluids, diffusion methods, methods and engineering

1 | INTRODUCTION

Lipid droplets (LDs) are cytosolic organelles composed of neutral lipids enclosed within a phospholipid monolayer. In healthy cells they are a source of energy, hormones, and secondary messengers, and they protect cells from lipotoxicity.¹ Abnormal formation of LDs has been associated with pathologies such as infection, inflammation, cancer and diabetes.² Numerous studies report that mobile LDs increase in number and size during apoptosis, but the cellular processes behind the production of LDs are not well understood.³

Apoptosis, a process often referred to as programmed cell death because of the regulated way in which the cells dies, requires the cell to maintain cellular energetics. It is a hallmark of cancer, as its impairment or absence leads to accumulation of cells that can become malignant.⁴ Since many cancer treatments are based on the induction of apoptosis in cancer cells, studying LD formation is useful in monitoring the effectiveness of cancer therapies.^{5,6}

Two methods commonly used to monitor the formation of LDs are NMR spectroscopy and fluorescence microscopy. NMR spectroscopy has been widely used to study the effects of apoptotic agents on the metabolic profiles of tissues and cell lines.⁷⁻⁹ In addition, ¹H MRS provides a non-invasive method for assessing tissue responses to cancer treatments *in vivo*.¹⁰ Solution-state ¹H NMR spectroscopy on cell or tissue extracts gives quantitative information on lipid concentration.^{11,12} In this case, the ¹H NMR spectra represent the collective signal from cytosolic LDs, lipids contained within cell organelles and membrane lipids. However, not all lipids may be extractable, depending on the extraction procedure used.

Visualization of intracellular lipids by fluorescence microscopy is possible by using lipid soluble dyes.¹³ It provides information on droplet size, number and localization in intact cells.¹⁴ In addition, live microscopy allows the measurement of diffusional mobility. However, several technical limitations prevent the study of LDs at the molecular level. These include resolution, photobleaching, long acquisition times and selective fluorescence labelling.

For *in vitro* NMR experiments, an increase in the lipid signal observed in ¹H NMR spectra has been linked to an increase in LD size as measured by microscopy.^{15,16} NMR-based measurements of the diffusion of mobile lipids have also been used to follow the size of LDs.¹⁷ *In vivo* measurements of apparent diffusion rates of mobile lipids in tissues have also been made, but these have not been specifically linked to droplet size previously.¹⁸ Diffusion experiments can be used to probe changes in LD size in intact cells and structural changes in cellular environment, such as viscosity of the cytosol or fluidity of cytoskeletal structures. Different types of macromolecule account for 20% to 40% of the free organelle volume of a cell,¹⁹ and along with cellular organelles and cell membranes restrict diffusion rates. For example, Griffin and colleagues reported that the apparent diffusion of intracellular water in endometrial cells was more than seven times slower than the diffusion of extracellular water.²⁰

In MRI, changes in apparent diffusion of water can be a sign of disease and it is a common clinical practice to use diffusion-weighted MRS for diagnostic purposes.²¹ Apparent diffusion measurements have also been used to probe LD behaviour *ex vivo*²² and *in vivo*.²³ However, few studies have focused on NMR-based diffusion rates of lipids in intact cells,^{17,20} because of the challenges of achieving the necessary spectral resolution in these media.

High-resolution magic angle spinning (HRMAS) ¹H NMR spectroscopy provides improved spectral resolution of heterogeneous biological samples.²⁴ It has been used to study lipid metabolism affected by a variety of diseases, for example cancer,²⁵ diabetes,²⁶ and schizophrenia,²⁷ as well as cellular processes such as apoptosis.²⁸ Furthermore, the lipid signals observed in HRMAS spectra of intact cells or tissue are from cytosolic LDs only, rather than lipids associated with membranes. As the dipole-dipole couplings are larger in cell membrane lipids, they are not resolved at the spinning speeds used in HRMAS ¹H NMR spectroscopy.²⁹ This is in contrast to solution state NMR spectroscopy of extracts where all lipid components are extracted.

In this study, we compare the metabolic response of intact cells treated with two apoptotic agents, cisplatin and etoposide, to that of a control group. Changes to lipid signals determined using HRMAS and solution state ¹H NMR spectroscopy are compared with standard assays for apoptosis and cell viability. In addition, we use HRMAS and solution-state ¹H NMR spectroscopy to study LDs in the control and treated cells and compare the results with those from fluorescence microscopy. We illustrate the advantages of using HRMAS ¹H NMR over solution-state ¹H NMR spectroscopy for the monitoring of apoptosis-related LD formation.

2 | METHODS

2.1 | General

All chemicals, unless otherwise stated, were purchased from Merck (Sigma Aldrich, Dorset, UK).

2.2 | Cell culture

The C2C12 cell line sub-cloned from a myoblast line established from normal adult C3H mouse leg muscle was cultured in Dulbecco's modified Eagle's medium (DMEM—D6429) containing 10% foetal bovine serum and 1% PenStrep (100 U mL⁻¹ penicillin + 100 µg mL⁻¹ streptomycin) in a humidified 5% carbon dioxide atmosphere at 37 °C. Cells were grown in T-75 culture flasks with filter-vented caps, seeded at approximately 1.5 × 10⁶ cells per flask. Myogenic differentiation was initiated upon reaching 60% confluence, by switching the cells to medium containing 2% horse serum supplemented with 1 µM insulin. After 5 days of differentiation, the cells were treated with apoptotic agents: cisplatin (60 µM final concentration) or etoposide (120 µM final concentration). Dimethyl sulfoxide (DMSO) was used as a vehicle for drugs and the equivalent volume was added to control cells (1% v/v). The cells were harvested with trypsin after 24 and 48 h incubation, frozen immediately in DMEM + 5% DMSO and stored at -80 °C until use.

2.3 | Cell viability

The trypan blue exclusion test was used to determine the number of viable cells present in cell suspensions before and after NMR experiments. The test was performed according to a standard cell counting protocol.³⁰ Briefly, 25 µL freshly harvested cells were transferred to a plastic vial and diluted with phosphate buffered saline (PBS; 1:5 dilution). An equal volume of 0.4% trypan blue dye (Sigma-Aldrich) was added to 8 µL cell suspension to obtain a 1:2 dilution and mixed by pipetting. The cell-dye mixtures (10 µL) were transferred to Countess cell counting chamber slides by placing the tip of the pipette at the notch. The viability of cell samples was measured with a Countess automated cell counter (ThermoFisher Scientific, Hemel Hempstead, UK). The total number of cells was used for normalization of the caspase 3 activity assay. Cell viability was expressed as a percentage of live cells. The viability of cells decreases in the MAS rotor by ~10% after 3.5 h data acquisition.

2.4 | Caspase 3 assay

Relative apoptosis levels in freshly harvested cell samples were measured using a Caspase 3 assay kit (Ac-DEVD-AMC, BD Pharmingen, San Diego, CA, USA) following the manufacturer's instructions. Briefly, reaction buffer containing Ac-DEVD-AMC was added to each cell lysate (10⁶ cells mL⁻¹) and incubated in a black 96-well microplate (Nunc, Thermo Fisher Scientific, Hemel Hempstead, UK) for 1 h at 37 °C in the dark. The fluorescence intensities were measured with a FLUOstar OPTIMA microplate reader (BMG LABTECH) at excitation/emission wavelengths of 380/420 nm.

2.5 | Lipid extraction

Thawed cells (5 × 10⁶ per sample) were washed with 5 mL PBS at room temperature. The metabolites and lipids were extracted simultaneously using a methanol/chloroform/water extraction method.³¹ Reagent-grade methanol and chloroform in a ratio of 2:1 (v/v; 500 µL) were added to each sample and the cells were briefly pulverized with a plastic pipette tip, vortexed and sonicated at room temperature for 1.5 h. Subsequently, Milli-Q water and chloroform in a ratio of 1:1 (v/v; 500 µL) was added, vortexed and sonicated again for 30 min. The two layers and cell pellet were separated by centrifuging (7,000 rpm, 7 min) and the lower chloroform fractions containing the cellular lipids were collected into glass vials. All solvents were then evaporated under a stream of dry nitrogen gas and the lipid fractions re-dissolved in 500 µL of chloroform-d + 0.05% (v/v) tetramethylsilane (TMS) (Cambridge Isotope Laboratories, Cambridge, MA) for NMR experiments.

2.6 | Solution NMR spectroscopy

¹H NMR spectra of lipid fractions from cell extracts were recorded on a Bruker AVANCE II + spectrometer (Bruker, Billerica, MA) operating at a frequency of 500.13 MHz and fitted with a 5 mm TXI probe. One-dimensional high-resolution ¹H NMR spectra were acquired at 300 K using a solvent suppression pulse sequence based on a one-dimensional NOESY pulse sequence (*noesypr1d*) to saturate the residual ¹H water signal. The experiments were run with four dummy scans and 128 acquisition scans with an acquisition time of 4.09 s, relaxation delay 2 s and mixing time of 80 ms. Total acquisition time was 13 min 48 s. 65.5k data points were recorded across a spectral width of 8012.82 Hz. A line-broadening apodization function of 0.3 Hz was applied to all ¹H NMR free induction decays, which were then pre-processed with an online tool—Workflow4Metabolomics (W4M) 3.0 (workflow4metabolomics.org).³² Lipid signal assignment was based on the previously reported chemical shifts for similar systems³³ and confirmed with two-dimensional ¹H-¹H correlation spectroscopy (COSY) (Supporting Information, Figures S1 and S2).

For the COSY, a standard Bruker pulse sequence (*cosygpprqf*) was used. A data matrix of 512×4096 points covering 8012×8012 Hz was recorded with 32 scans for each increment and a relaxation delay of 2 s. Spectra were Fourier transformed with sine-bell functions and 0.3 Hz (F1) and 1 Hz (F2) exponential and 0.1 Hz Gaussian (F1 only) effective line broadening functions applied. All chemical shifts were referenced with respect to TMS at 0 ppm.

2.7 | High-resolution magic angle spinning NMR (HRMAS NMR) spectroscopy

Thawed cells (5×10^6 per sample) were washed in deuterated PBS. Cell pellets were combined with 10 μ L deuterated phosphate-buffered saline + 0.05 mM trimethylsilylpropanoic acid (TSP; Cambridge Isotope Laboratories) and packed into 4 mm zirconium oxide rotors with 50 μ L Kel-F inserts (Bruker). All measurements were carried out at 300 K and 5 kHz spinning rate on a 500.13 MHz NMR Bruker AVANCE II+ spectrometer equipped with a 4 mm HR-MAS probe with a gradient coil allowing gradient pulses up to 34 G cm^{-1} . The temperature was allowed to stabilize for 5 min before acquiring the data. The temperature remained within ± 1 K of the set temperature during acquisitions. One-dimensional high-resolution T_2 -edited Carr-Purcell-Meiboom-Gill (CPMG) ^1H NMR spectra were acquired using pulse sequences with continuous wave solvent presaturation (*cpmgpr1d*). All experiments were run with 4 dummy scans and 64 acquisition scans with an acquisition time of 5.45 s and relaxation delay of 4 s. 65.5k data points were recorded across a spectral width of 6009.615 Hz. For the acquisition of CPMG spectra, total spin-spin relaxation delay ($2n\tau$) of 40 ms was used, where spin echo number $n = 20$ and spin echo time $\tau = 1$ ms. Total acquisition time was 10 min 48 s. A line-broadening apodization function of 1.0 Hz was applied to all HRMAS ^1H NMR free induction decays prior to Fourier transformation. All FIDs were pre-processed with W4M 3.0. Lipid signal assignment was based on literature chemical shifts for similar systems.^{20,34}

Two-dimensional diffusion spectra (diffusion-ordered spectroscopy, DOSY) were recorded using the longitudinal eddy current delay bipolar gradient pulse sequence (*ledbpgp2s*)³⁵ with a diffusion delay (Δ) of 0.05 s, a diffusion-encoding pulse width (δ) of 2 ms, echo time of 2.2 ms, and gradient strengths increasing from $b = 124$ to $1,571 \text{ s mm}^{-2}$ in 16 linear steps. At each gradient strength, 32 scans and 65.5k data points were acquired with an acquisition time of 5.45 s, a relaxation delay of 4.0 s, and a line broadening of 1 Hz. The total acquisition time was 1 h 23 min. Manual phasing and baseline correction was applied before peak-picking in Dynamics Centre (Bruker). All spectra were acquired with constant receiver gain value and normalized to total spectral integrals.

2.8 | High-gradient diffusion NMR spectroscopy

Thawed cells (1×10^7 per sample) were washed in deuterated PBS. Cell pellets were resuspended in 100 μ L PBS containing D_2O + 0.05 mM TSP and packed into 3 mm inserts. All measurements were carried out at 300 K on a Bruker Avance IIIHD 400 MHz NMR spectrometer fitted with a 5 mm Diff50 z-diffusion probe for a wide bore magnet, comprising an actively shielded Z-gradient with strengths up to $50 \text{ G cm}^{-1} \text{ A}^{-1}$ (up to 2800 G cm^{-1}). DOSY spectra were recorded using the same pulse sequence and diffusion parameters as for the HRMAS NMR experiments. The gradient strength was increased from $b = 6$ to $420 \text{ 951 s mm}^{-2}$ in 256 linear steps. For each gradient strength, 32 scans and 50k data points were acquired with an acquisition time of 5.21 s, a relaxation delay of 0.5 ms, and a line broadening of 1 Hz. Manual phasing and baseline correction was applied before peak-picking in Dynamics Centre (Bruker).

2.9 | Cell preparation and confocal microscopy imaging

After the apoptotic treatment, the differentiated myotubes (5×10^4 cells mL^{-1}) were transferred onto 35 mm glass base collagen-coated dishes (Nunc, Thermo Fisher Scientific) and left to attach overnight. The samples were incubated with 1 mL staining solution (50 $\mu\text{g mL}^{-1}$ boron dipyrromethene (BODIPY) in PBS) for 10 min in the dark, washed with PBS twice before being observed under a microscope, and photographed. Images were acquired on a Leica TCS SP8 confocal microscope using a 1.3 NA, 63 \times oil immersion objective lens, a scan speed of 400 Hz and a line averaging of 2. Multichannel imaging was performed on a $100 \mu\text{m} \times 100 \mu\text{m}$ area (sampled at 1024×1024 pixels) using an excitation laser line of 488 nm (emission detection 500–520 nm). 2D time-lapse sequences were taken every 5 s, resulting in 50–60 images of a $50 \times 50 \mu\text{m}^2$ area (2048×2048 pixels).

2.10 | Data analysis

1D ^1H NMR spectra were analysed over the spectral region between 0.5 and 8.0 ppm, with the exclusion of the water region (4.5–5.0 ppm), and normalized to the sum of all peak integrals using MetaboAnalyst v. 4.0 (University of Alberta, Canada).³⁶ The changes in lipid integrals induced on the treatments are reported as a fold change relative to the control group.

Diffusion data was fitted using Dynamics Centre v2.5.1 (Bruker). The relative standard deviations of all diffusion fits to exponential decays were less than 5%. The minimum signal-to-noise ratio for the highest b -values was 21.3 (Supporting Information, Tables S1 and S2). The contribution of non-lipid metabolites to apparent diffusion coefficients of mobile lipids is excluded by taking advantage of the significant difference between the apparent diffusion coefficients of lipids and non-lipid metabolites (Supporting Information, Figure S5).

Image analysis and measurements were carried out using the ImageJ software package v. 1.52i (National Institutes of Health, Bethesda, MD, USA). The results were averaged across 548, 1183, and 560 LDs in control, cisplatin, and etoposide samples, respectively. Time-lapse images were pre-processed to extract object characteristics and trajectories using standard image processing techniques and tracking algorithms from the TrackMate plugin (ImageJ).³⁷

Statistical analysis was carried out in Excel (Microsoft, Seattle, WA) or MetaboAnalyst; Student's unpaired t test with equal variance was used to compare two groups. Analysis of variance (ANOVA) with the post hoc Fisher least significant difference analysis was used when multiple comparisons were made. Unless otherwise stated, data are presented as mean \pm standard error of the mean (SEM) and represent a biological variance of at least four repeats. False discovery rate adjusted p values less than 0.05 were considered significant. For curve and line fitting, partial least-square regression was used. Mean square displacement analysis was based on NMR diffusion data and calculated from the following equation: $\langle x^2 \rangle = 2Dt$, where $\langle x^2 \rangle$ is the mean square displacement, D the diffusion rate measured by NMR, and t the diffusion time (50 ms).

3 | RESULTS AND DISCUSSION

3.1 | LD concentration determined by NMR spectroscopy and the link to apoptosis

C2C12 mouse myotubes were subjected to two apoptosis-based treatments commonly used in cancer therapies: cisplatin or etoposide. We compared ^1H HRMAS NMR spectroscopy analysis of lipids in intact cells with solution-state ^1H NMR of lipid extracts from the whole cells after incubation for 48 h. The HRMAS spectrum of intact cells represents total NMR-detectible metabolites with relatively fast tumbling rates, and for example included resonances from glucose, lactate, creatine, and lipids. Solution-state ^1H NMR of lipid extracts, on the other hand, represent all extracted lipids including membrane lipids, which are not visible in the HRMAS ^1H NMR spectra. Figure 1A and 1B shows NMR spectra of intact cells and the hydrophobic (lipid) fraction of cell extracts. We assigned lipid signals in control and treated samples, and compared lipid content across the two NMR techniques. Figure 1C-F shows the results for $-\text{CH}_3$ and $-\text{HC}=\text{CH}-$ resonances.

Both NMR methods showed a significant increase in lipid $-\text{CH}_3$ signal intensities for apoptotic cells. The HRMAS ^1H NMR spectrum showed a 100% increase in the intensity of the lipid $-\text{CH}_3$ signal, whereas solution ^1H NMR showed only a 10% increase. Unsaturated lipids increased by 100% following etoposide treatment in HRMAS NMR spectroscopy spectra and by 50% in solution-state NMR, but no change was seen for cisplatin treated cells by solution state NMR. The data showed that the increase of NMR-visible lipids during apoptosis is larger as detected by HRMAS ^1H NMR spectroscopy. This discrepancy between cell extract and intact cell samples suggests two processes may be occurring to induce these lipid changes: (1) a modest increase in de novo lipogenesis, which is detected by both solution state and HRMAS ^1H NMR spectroscopy; and (2) a larger effect associated with changes in the biophysical properties of NMR-observable lipids, which may be associated with partitioning of lipids from the cell membrane to LDs and/or changes in LD size. Both processes may affect the tumbling rate of lipids, increasing the NMR visibility of the resonances associated with fatty acids.

Solution-state NMR spectra of whole cell extracts represent the collective signal from cytosolic LDs, membrane lipids, and lipids contained within cell organelles. The change in LD-associated lipid concentration is 'masked' due to opposing changes in phospholipids during apoptosis. Cells undergoing apoptosis are characterized not only by increased mobile lipid profiles, but also by decreased phosphatidylcholine and total phospholipid concentration as reported by Gibbons and colleagues.^{38,39} In order to determine changes in mobile lipids using a solution NMR approach, LDs need to be isolated first. This is a time and labour expensive process and not all lipids may be extracted. The data suggest that HRMAS NMR offers an improved way to monitor changes in mobile lipid concentration in intact cells as it is more selective.

Cellular and biochemical changes during apoptosis can also contribute to the increases in NMR-visible lipids in intact cells. Quintero and colleagues reported an increase in NMR-visible lipids during cell proliferation but no absolute increase in neutral lipids, and proposed an increased transport of TAG as a possible explanation.⁴⁰ It is also possible that cytoskeletal remodelling during apoptosis leads to increased LD mobility, which makes them more NMR visible.⁴¹

In order to confirm the level of apoptosis in the control and treated cells they were tested after 8, 24, and 48 h incubation using the caspase 3 assay. Figure 2A shows the fold change during apoptosis relative to the control group for different incubation periods. The samples incubated with cisplatin and etoposide for 24 h and 48 h exhibited significantly higher levels of apoptosis compared with the control group. Figure 2B shows a positive correlation between apoptosis levels and the NMR-visible lipid signal in intact cells ($R^2 = 0.86$ for pooled samples, $n = 36$). This is consistent with the previous reports of LDs as a biomarker for apoptosis^{3,7} and confirms apoptosis-related lipid accumulation.

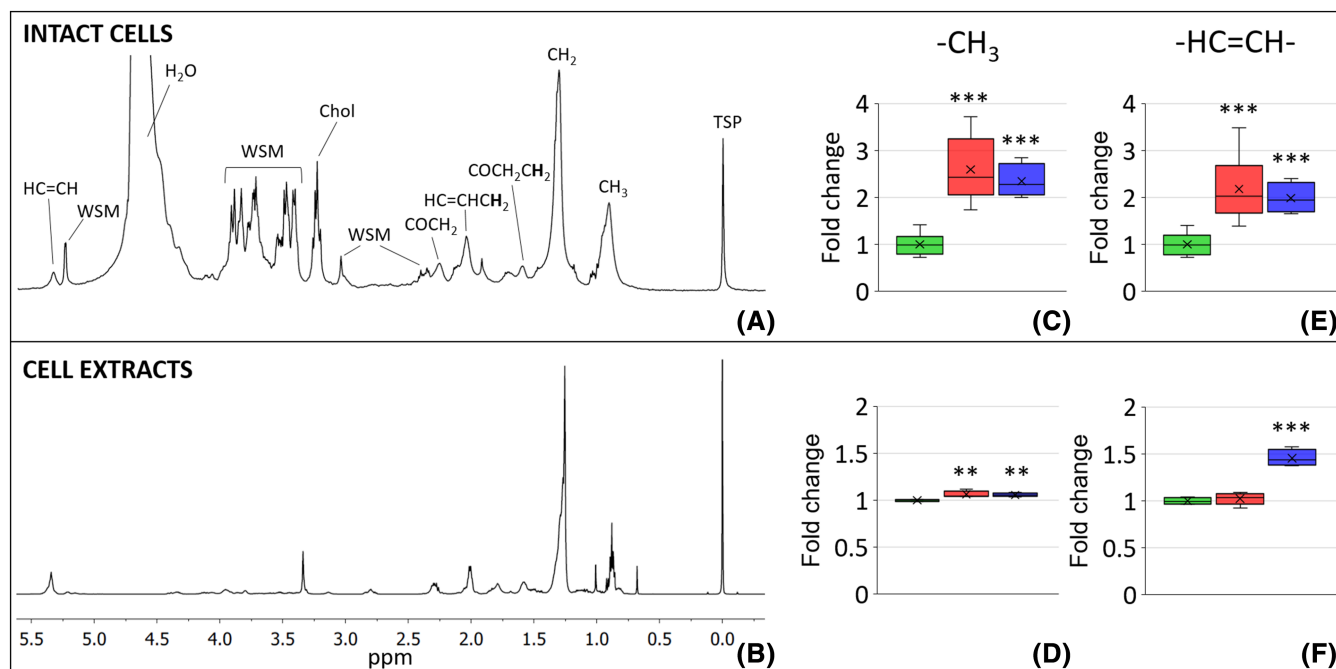


FIGURE 1 Comparison of metabolic profiles of intact cells recorded by HRMAS ^1H NMR and cell extracts recorded by solution ^1H NMR spectroscopy. A, Representative 1D ^1H NMR spectra of intact cells in PBS containing D_2O + 0.05 mM TSP; B, hydrophobic fraction of cell extracts in chloroform- d + 0.05% v/v TMS. Lipid signals were assigned based on literature values and COSY ^1H - ^1H experiments. WSM, water-soluble metabolites; Chol, choline compounds. C-F, The fold changes in $-\text{CH}_3$ and $-\text{HC}=\text{CH}-$ lipid signal intensities are shown as box and whisker plots for intact cells (C, E) and cell extracts (D, F) for control (green), cisplatin (red) and etoposide (blue) treated cells for 48 h. The boxes show median concentrations and the 25th and 75th percentiles; the whiskers indicate minimum and maximum concentrations. Data normalized to total spectral intensity. ** $p < 0.01$, *** $p < 0.001$, $n = 4$

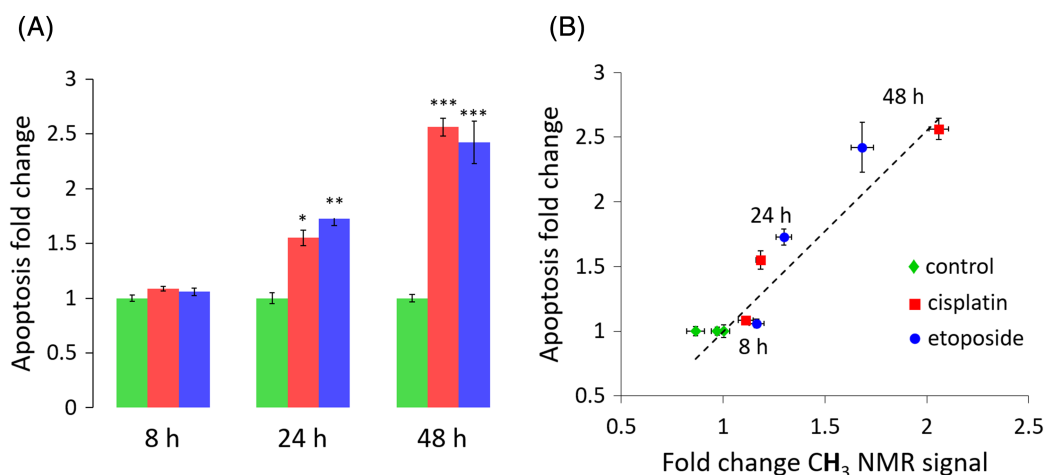


FIGURE 2 Apoptosis in cultured mouse C2C12 myotubes exposed to cisplatin, and etoposide for 8 h, 24 h, and 48 h compared with the control group. A, Fold change in apoptosis relative to the control group measured with the caspase 3 fluorometric assay. * $p < 0.05$, ** $p < 0.01$, *** $p < 0.001$. B, The correlation between apoptosis level and NMR lipid signal for the control and treated samples at 8 h, 24 h, and 48 h. Error bars indicate standard error, $n = 4$

3.2 | Determination of apparent diffusion of mobile lipids in intact cells by HRMAS NMR

The increased lipid signal intensities observed in the NMR spectra can be associated with either the formation of larger LDs or a higher number of small LDs. We measured apparent diffusion coefficients of mobile lipids by DOSY under HRMAS to discriminate between these two scenarios. The apparent diffusion coefficients of the five lipid signals and choline-containing compounds assigned in Figure 1 are shown in Table 1.

TABLE 1 Mean diffusion coefficients of selected lipid signals for control, cisplatin-, and etoposide-treated samples after 48 h. Control and cisplatin $n = 8$, etoposide $n = 4$. Statistical significance was determined with ANOVA, $*p < 0.05$. The apparent diffusion coefficient values were measured at a diffusion time of 50 ms. \pm values refer to standard error

Lipid peak	Control [$\mu\text{m}^2 \text{s}^{-1}$]	Cisplatin [$\mu\text{m}^2 \text{s}^{-1}$]	Etoposide [$\mu\text{m}^2 \text{s}^{-1}$]
-CH ₃	148.1 \pm 22.4	72.2 \pm 9.1	113.2 \pm 22.2
-CH ₂ -	120.1 \pm 14.0	67.4 \pm 8.6*	102.6 \pm 18.1
-HC=CHCH ₂ -	125.2 \pm 7.1	76.1 \pm 8.3*	104.5 \pm 21.9
-COCH ₂ -	125.4 \pm 7.9	71.5 \pm 8.5*	103.4 \pm 21.5
-HC=CH ^a	91.1 \pm 27.4	69.5 \pm 8.7	117.1 \pm 44.6
choline	164.7 \pm 12.1	217.3 \pm 22.2	146.3 \pm 21.8

^aThe proximity of the HC=CH lipid signal to the water signal means that the optimization of water suppression is crucial to obtain accurate and reproducible values for this signal.

In order to highlight the differences between control and treated samples we analysed the diffusion data using principal component analysis (PCA) (Figure 3A) and ANOVA (Figure 3B).

The diffusion data derived from DOSY NMR experiments were subjected to multivariate statistical analysis in MetaboAnalyst. PCA was used to observe inherent clustering and to discriminate the variables that are responsible for variation between the groups (Figure 3A). Group separation along principal component 1 (PC1) accounted for 67.3% of total variation and PC2 accounted for 24.2%. Three apparent diffusion coefficients showed significant discriminative power between control and cisplatin samples: -CH₂-, -HC=CHCH₂-, and -COCH₂-. The cisplatin group was characterized by the decreased apparent diffusion coefficients of lipids. The apparent diffusion coefficients measured for the etoposide samples also showed a decreasing trend, albeit not significant.

An ANOVA analysis allows us to highlight differences between cisplatin, etoposide, and control samples. In the cisplatin treated samples, the -CH₂-, -HC=CHCH₂-, and -COCH₂- signals gave significantly lower rates (Figure 3B). Griffin and colleagues have previously reported values for apparent diffusion rates of lipids in intact endometrial cells measured by HRMAS ¹H NMR spectroscopy.²⁰ The comparison of the apparent diffusion rates is shown in Table 2. Those for -CH₃-, -CH₂-, and choline compounds showed good agreement, whereas those for -HC=CHCH₂-, -COCH₂-, and -HC=CH- are much higher in endometrial cells. This may be due to overlap of different peaks in the NMR spectrum and differences in metabolic profiles of different cell lines.

The content and concentration of small metabolites and lipids vary from cell line to cell line. The NMR region of 2.0-2.5 ppm, which corresponds to -HC=CHCH₂- and -COCH₂- lipid signals, is crowded with peaks from other small metabolites such as acetyl groups and glutamate, which diffuse much faster. The contribution of these metabolites results in higher apparent diffusion rates for lipids and it is important to exclude

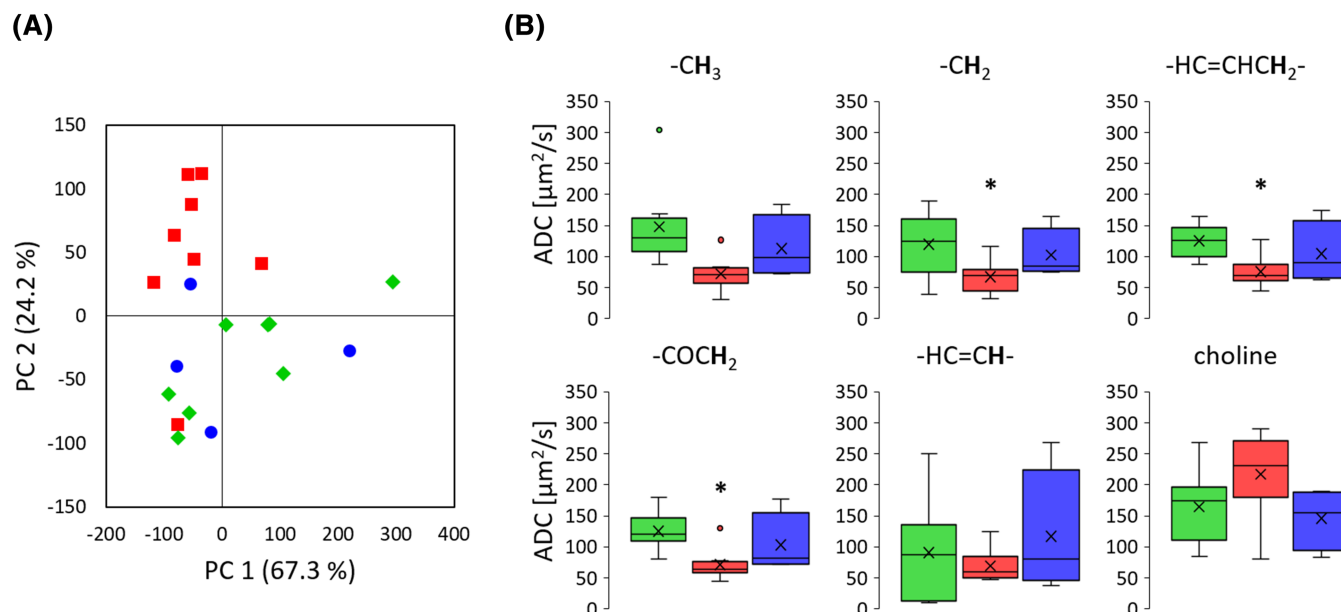


FIGURE 3 Statistical analysis of NMR-based diffusion data of intact cells: control (◆, green), cisplatin (■, red), and etoposide (●, blue). A, Two-dimensional PCA score plot derived from the diffusion rates of six lipid species. Each data point represents one sample. B, Box and whisker plots comparing apparent diffusion coefficients (ADCs) for each lipid signal across control, cisplatin, and etoposide. The box covers the 25th and 75th percentiles, the line in the box represents the median value, the cross represents mean and the whiskers indicate minimum and maximum values. Outliers are shown as points. Significant perturbation assessed by ANOVA: $*p < 0.05$

them. This was achieved by starting the diffusion experiment at a non-zero gradient value ($b = 124 \text{ s mm}^{-2}$). Moreover, the chemical groups under investigation belong to a series of different fatty acids, which in turn can be on different lipids, eg FFAs, TAGs, and phosphocholines, and these will have different mobilities. NMR DOSY spectroscopy measures an average apparent diffusion coefficient across the whole ensemble.

Apparent diffusion coefficients of mobile lipids have also been measured *ex vivo* by ^1H MRS.¹⁸ Remy et al reported two values of apparent diffusion coefficients for mobile lipids in rat glioma: $46 \pm 17 \mu\text{m}^2 \text{ s}^{-1}$ for the mean LD radius of $0.485 \mu\text{m}$ and $11.0 \mu\text{m}^2 \text{ s}^{-1}$ for an equivalent spherical diameter of $4.27 \pm 0.71 \mu\text{m}$.⁴² The discrepancy between these two measurements was explained by differences in the range of gradient strengths and differences in tumour growth. The higher value was measured with $b = 0\text{--}8000 \text{ s mm}^{-2}$ and the slower rate with $b = 0\text{--}50\,000 \text{ s mm}^{-2}$. Our apparent diffusion rates from intact cells are expected to be faster because of the structure of the samples (cell versus tissue) and relatively low gradient strengths used ($b = 124\text{--}1571 \text{ s mm}^{-2}$). In order to explore this large difference in apparent diffusion rates we have investigated a wider range of gradient strengths than has been used previously.

We have investigated the impact of gradient strength using a high gradient diffusion probe (Diff50, $b = 6\text{--}420\,951 \text{ s mm}^{-2}$). A larger range of gradient strengths enables us to better investigate lipids diffusing at slower rates. Figure 4 shows a Stejskal-Tanner plot generated using this wide range gradient approach.⁴³ We explored fitting the data to single- and biexponential models but neither described the data satisfactorily. The solid line presented in Figure 4 shows the fit using a three-component model, which provided the best fit to the diffusion data. The fastest apparent diffusion rate measured using the high-gradient-strength probe is similar to the apparent diffusion coefficients measured by HRMAS NMR. The apparent diffusion values for the $-\text{CH}_2$ lipid signal are $120.1 \mu\text{m}^2 \text{ s}^{-1}$ and $175.8 \mu\text{m}^2 \text{ s}^{-1}$ as measured with the HRMAS probe and the Diff50 probe, respectively. Using the higher gradient strength, we are now able to resolve two other lipid species with apparent diffusion rates of $41.7 \mu\text{m}^2 \text{ s}^{-1}$ and $0.582 \mu\text{m}^2 \text{ s}^{-1}$.

We compared apparent diffusion rates of lipids in intact cells measured using HRMAS and solution-state NMR. These measurements show that HRMAS NMR and solution diffusion measurements give similar results regardless of sample packing (rotor versus 3 mm tube) and experimental conditions (spinning versus no spinning). In addition, there are lipids diffusing more slowly in intact cells, which cannot be studied with standard

TABLE 2 Mean apparent diffusion coefficients of selected lipid signals for untreated muscle cells and endometrial cells as reported by Griffin et al and for rat glioma tissue by Remy et al. \pm values refer to standard error, *value corresponds to restricted diffusion

Lipid peak	C2C12 muscle cells [$\mu\text{m}^2 \text{ s}^{-1}$]	Endometrial cells ²⁰ [$\mu\text{m}^2 \text{ s}^{-1}$]	Rat glioma tissue ¹⁸ [$\mu\text{m}^2 \text{ s}^{-1}$]
$-\text{CH}_3$	148.1 ± 22.4	200 ± 10	
$-\text{CH}_2-$	120.1 ± 14.0	200 ± 10	$46 \pm 17^*$
$-\text{HC}=\text{CHCH}_2-$	125.2 ± 7.1	600 ± 40	
$-\text{COCH}_2-$	125.4 ± 7.9	800 ± 50	
$-\text{HC}=\text{CH}-$	91.1 ± 27.4	500 ± 30	
Choline	164.7 ± 12.1	200 ± 10	

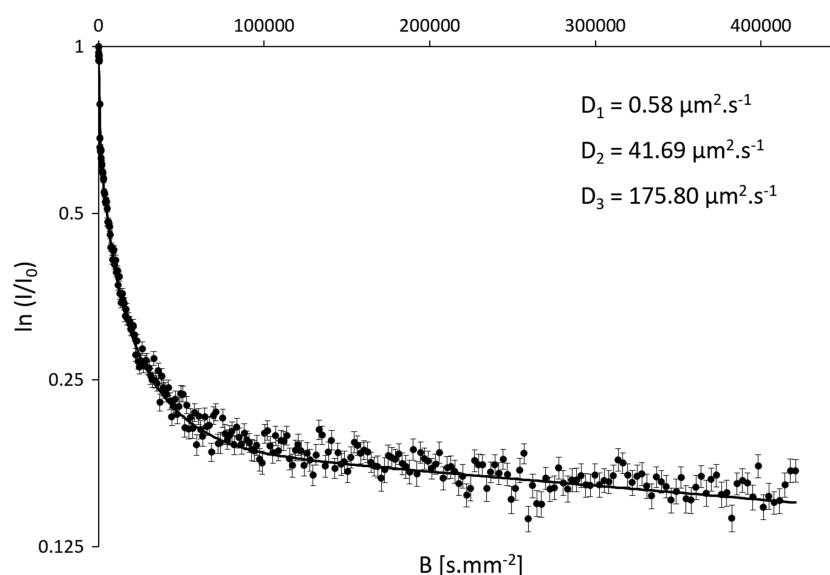


FIGURE 4 A triexponential diffusion fit for the CH_2 signal displayed as a Stejskal-Tanner plot. Diffusion data collected for untreated cells packed in 3 mm tubes using a high gradient 5 mm probe (Diff50). Error bars correspond to the line fitting errors

NMR probes. Slower moving lipid species may correspond to lipids located in different cellular environments (for example, the viscosity and molecular crowding is different in nucleus and cytoplasm^{44–46}) or even in lipid rafts, where the movement of lipids is highly restricted.⁴⁷ This approach opens up new opportunities for investigating lipid behaviour in intact cells.

3.3 | Microscopy compared with HRMAS ¹H NMR spectroscopy of mobile lipids

The standard approach for measuring the size of LDs in intact cells is fluorescence microscopy. Figure 5A–C shows images of labelled LDs in control and treated cells. The size of LDs was determined by image analysis.

The analysis of the LD populations showed that the average LD cross sectional areas was $0.26 \pm 0.03 \mu\text{m}^2$, $0.40 \pm 0.03 \mu\text{m}^2$, and $0.36 \pm 0.04 \mu\text{m}^2$ in the control, cisplatin, and etoposide-treated samples, respectively. Of these, only the size of LD in cisplatin samples was confirmed to be statistically significant for the group differentiation over all samples ($p = 0.04$, ANOVA).

We compared HRMAS ¹H NMR-based diffusion coefficients with the size of LDs measured by fluorescence confocal microscopy. LD size is inversely related to diffusion coefficient as described by the Stokes-Einstein equation given below:

$$D = \frac{kT}{6v\pi} \left(\frac{1}{r} \right) \quad (1)$$

where D is the diffusion constant [$\text{m}^2 \cdot \text{s}^{-1}$], k Boltzmann's constant [$\text{m}^2 \cdot \text{kg} \cdot \text{s}^{-2} \cdot \text{K}^{-1}$], T temperature [K], v viscosity [$\text{kg} \cdot \text{m}^{-1} \cdot \text{s}^{-1}$], and r the radius of the diffusing particle [m].

Figure 5D shows a plot of the apparent diffusion coefficients determined by HRMAS NMR against LD size from microscopy. The apparent diffusion coefficients for the individual lipid signals, $-\text{CH}_3$, $-\text{CH}_2$, $-\text{HC}=\text{CHCH}_2$, $-\text{COCH}_2$, and $-\text{HC}=\text{CH}$ (Table 1), correlated with the mean LD

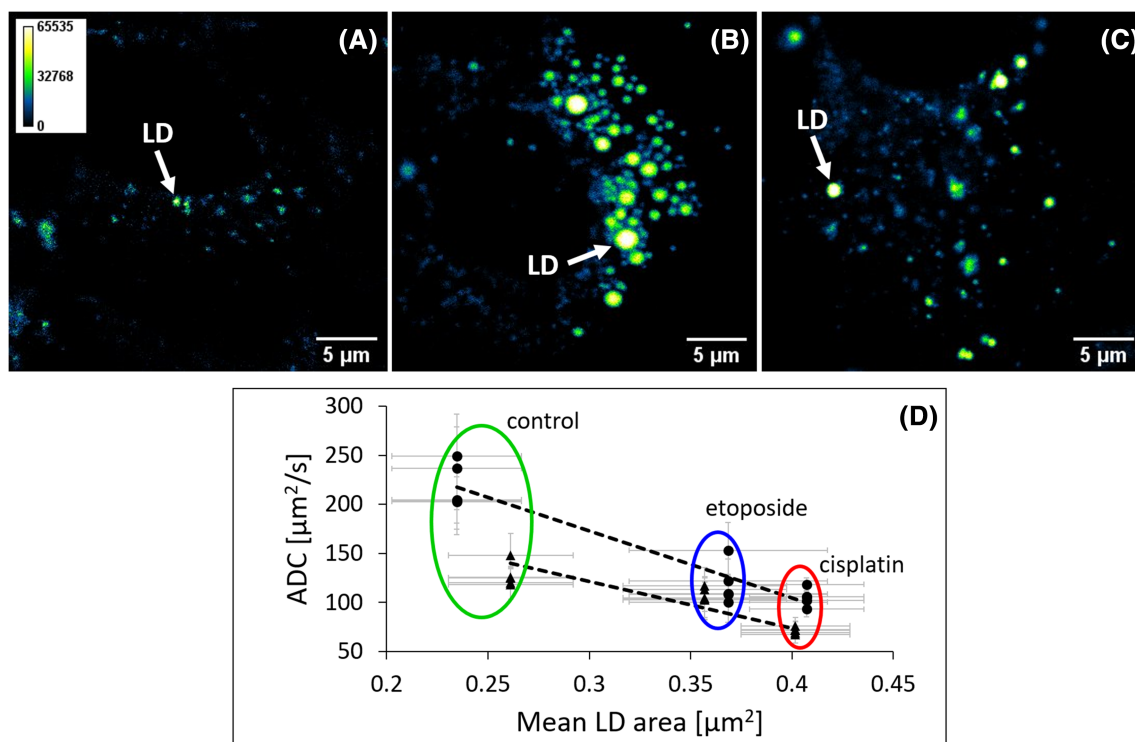


FIGURE 5 Correlation of microscopy-based LD size estimates and HRMAS ¹H NMR-based mean apparent diffusion coefficients. A–C, Representative images of fluorescence labelled LDs in a single cell: A, control; B, cisplatin treatment; C, etoposide treatment. Arrows indicate neutral lipids in LD stained with BODIPY dye. Images were taken after 48 h incubation. D, Regression analysis for mean LD size and NMR-based diffusion rates for control, cisplatin, and etoposide samples at 24 h (●) and 48 h (▲) incubation times. Four dots aligned vertically represent four chemical groups (CH_3 , CH_2 , COCH_2 , $\text{CH}=\text{CHCH}_2$, also shown in Supporting Information, Figure S3). The graph represents the collective apparent diffusion coefficient from each chemical group. Error bars indicate the standard error. Separate regression fits for the two incubation times are shown ($R^2 = 0.897$ for 24 h and $R^2 = 0.921$ for 48 h)

area. The experimental data from the 24 h and 48 h time points were fitted using two separate regression models. In both cases the data are highly correlated ($R^2 = 0.90$ for 24 h and $R^2 = 0.92$ for 48 h)

From Figure 5D we can see that the apparent diffusion coefficients from HRMAS NMR correlate well with LD size estimated by microscopy. The results illustrate that NMR-based diffusion measurements can differentiate between normal and apoptotic cells and could therefore have potential application in monitoring LD size during apoptotic-based treatments in intact cells.

3.4 | Viscosity of cytoplasm

Since LD size by microscopy and mobile lipid diffusion by NMR spectroscopy were highly correlated, we investigated if combining the HRMAS ^1H NMR diffusion data and fluorescence microscopy measurements would lead to correct estimation of the cytoplasmic viscosity. If we assume that LDs are ideal spheres, a constant temperature (300 K), and no cytoplasmic changes due to treatments, we can deduce the viscosity from the modified Stokes-Einstein equation as shown in Equation 2.

$$D = b + \frac{kT}{6\nu\pi} \left(\frac{1}{r} \right) \quad (2)$$

where b is a constant [$\text{m}^2 \cdot \text{s}^{-1}$].

The viscosity can be determined from the slope of the graph of $D_r^{\frac{1}{2}}$. Using data described in Figure 5D, we calculated cytoplasmic viscosity. The values obtained for each lipid signal and their average are listed in Table 3 and the $D_r^{\frac{1}{2}}$ graphs for each lipid signal are in the Supporting Information.

The intracellular viscosity values reported in various cell lines and by different methods vary widely: 0.75–18 mPa s at 300 K.⁴⁹ Our viscosity values calculated based on NMR diffusion data are in agreement with values from Ye et al, who reported the viscosity of cytosol as 1.7–2.55 mPa s measured by ^{19}F NMR spectroscopy.⁴⁸ Moreover, the viscosity calculated for cells incubated for 24 h is significantly different from the viscosity of cells incubated for 48 h ($p = 0.01$). The different values of viscosity for 24 h and 48 h samples may be explained by cytoplasmic changes during cell maturation/cell growth. Changes in the cytoplasmic viscosity have been reported during germination⁵⁰; and the cytoplasm viscosity is sensitive to changes in concentration of Ca^{2+} , Mg^{2+} , and ATP.⁵¹ This suggests that, HRMAS NMR-based diffusion measurements may be able to detect not only changes in mobile lipids but also changes in cytosol viscosity. Further experiments are also needed to understand the impact of the freeze-thaw cycle on cytosolic viscosity.

3.5 | Determination of mean displacement

In addition to measuring LD size by microscopy we also tracked the movement of individual LDs in intact cells for the control and cisplatin samples. By tracking individual LDs, we were able to calculate mean square displacement and compare it with the value determined by HRMAS ^1H NMR diffusion measurements. Equation 3 describes the relationship between one dimensional diffusion and mean square displacement.⁵²

$$\langle r \rangle^2 = 2Dt. \quad (3)$$

Figure 6A shows a comparison between LD mean displacement values calculated from NMR diffusion data and mean displacements measured by microscopy tracking. Both the microscopy-based and NMR-based mean square displacements were shorter for cisplatin than for the control group, which is consistent with larger LDs that diffuse more slowly. However, the microscopy-based mean displacements were shorter than the NMR-based mean displacements.

TABLE 3 The viscosity (ν) of cytoplasm calculated from HRMAS ^1H NMR diffusion data and fluorescence microscopy for cells at 24 h and 48 h incubation time points. For comparison, we included values of cytoplasm viscosity measured using T_1 relaxation times of ^{19}F -labelled proteins in cells by ^{19}F NMR spectroscopy⁴⁸

Lipid signal	ν 24 h [mPa·s]	ν 48 h [mPa·s]	ν ^{19}F [mPa·s]
-CH ₃	1.75	2.13	
-CH ₂ -	1.37	3.20	
-HC=CHCH ₂ -	2.04	3.33	
-COCH ₂ -	1.97	3.05	
Average	1.74 ± 0.13	2.93 ± 0.24	1.7-2.55

It is interesting to discuss the discrepancy between the results, as the two methods have different spatial and temporal detection limits. The spatial resolution of the microscopy used here allows monitoring of apparent LD diffusion.⁵³ Conversely, HRMAS NMR-based diffusion experiments in our study describe mobility of LD-associated lipid molecules. Therefore, apparent diffusion coefficients and hence mean displacements measured by the two methods correspond to different biological processes: microscopy captures decreased apparent diffusion rates in apoptotic cells due to larger LDs, and HRMAS NMR spectroscopy most likely captures decreased apparent diffusion rates of mobile lipids, which can be linked to the more crowded environment within larger LDs.

Our results are in contrast to the study by Pérez and colleagues, who reported similar sizes of LDs obtained from microscopy and NMR experiments.¹⁷ Following the same approach (diameter = mean displacement $\times \sqrt{10}$), we calculated the mobile lipid compartment sizes based on NMR mean displacement and obtained the values of 5.9 μm and 4.22 μm for control and cisplatin, respectively. The results suggest that our NMR experiment does not measure the changes in LD size per se, but the changes in mobility of lipids within LDs.

In addition, other subcellular organelles can contribute to the NMR-based mean square displacement values, such as small endosomes. Martín-Sitjar and colleagues reported that increasing MAS spinning rate resulted in reversible increased in the NMR-visible lipid resonances, and attributed this to the fatty acyl chains of phospholipids in intracellular endosomes.⁵⁴ Indeed, we also detected an increase in the choline-containing compounds (3.21–3.28 ppm, Supporting Information, Figure S4), which supported endosomal phospholipid detection by HRMAS NMR spectroscopy. The viability of cells decreased in the MAS rotor by $\sim 10\%$ after the data acquisition, while this is not the case during the microscopy experiment. This could be another potential explanation for the discrepancy.

From a temporal perspective, NMR measures diffusion on a millisecond time scale (50 ms), while microscopy measures diffusion on a second time scale (5–6 s). This difference in observation time means that NMR-based diffusion measurements may be less sensitive to restricted diffusion. We tested if NMR-based diffusion rates correspond to free or restricted diffusion by running variable diffusion time NMR experiments over the range of 50–700 ms. The results in Figure 6B show that the apparent diffusion coefficients of mobile lipids in both control and treated cells decrease with increasing diffusion time, which is characteristic for restricted diffusion.⁵⁵ The data are described well by single-exponential fits. For free diffusion we expect a constant value of diffusion coefficients regardless of diffusion time.⁵⁶ For the diffusion data presented in Figure 6A the diffusion time was 50 ms. During this time, lipid molecules travel an average distance of 3.5 μm (Equation 3), and are prone to collisions with the compartment boundary and collisions with other molecules. While there is a clear difference in LDs between control and apoptotic samples regardless of analytical method used, more experiments are needed to investigate the reasons for the relationship between the size of LDs and NMR-based diffusion measurements.

3.6 | Conclusions

HRMAS ^1H NMR spectroscopy showed differences in the lipid profiles of control cells and those treated with cisplatin and etoposide. The concentration of NMR-visible lipids increases on treatment and it correlates well with the degree of apoptosis as measured by the caspase assay. Diffusion data showed significant decrease in apparent diffusion rates of NMR-visible lipids at 50 ms diffusion time upon apoptosis, and this correlated well with an increase in LD size measured with fluorescence microscopy. High-gradient-strength diffusion experiments revealed a broader range of diffusion environments than are seen by standard techniques. Microscopy and NMR spectroscopy-based mean displacements are shorter for cisplatin-treated cells compared with controls.

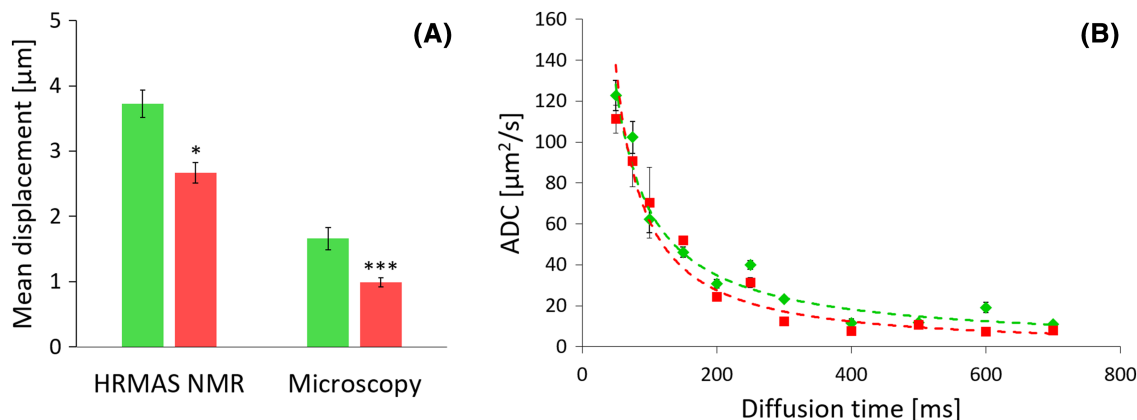


FIGURE 6 A, Mean and SEM values of LD displacement calculated from HRMAS ^1H NMR diffusion data and confocal fluorescence microscopy. B, Apparent diffusion coefficients of LDs in intact cells as a function of diffusion time. Data correspond to control (\blacklozenge , green) and cisplatin (\blacksquare , red) treated cells at 24 h. Error bars correspond to standard errors; asterisks represents statistical significance: * $p < 0.05$, *** $p < 0.001$

HRMAS NMR spectroscopy offers a label-free approach for monitoring changes in lipid behaviour during apoptosis, and could provide a minimally invasive technique for monitoring this molecular event in vitro and in vivo.

ACKNOWLEDGEMENT

We thank Dr Robert Shaw for useful discussions about statistical analysis and Cambridge Advanced Imaging Centre for access to the microscopy facility. This work was supported by EPSRC, MRC, and Astra Zeneca.

FUNDING INFORMATION

Work in the JLG laboratory is sponsored by the Medical Research Council (MRC) (MR/P011705/1). MW is sponsored by an Engineering and Physical Sciences Research Council (EPSRC) ICASE studentship in conjunction with Astra Zeneca (Studentship Reference 1 789 837).

ORCID

Julian L. Griffin  <https://orcid.org/0000-0003-1336-7744>

REFERENCES

1. Wang CW. Lipid droplets, lipophagy, and beyond. *Biochim Biophys Acta–Mol Cell Biol Lipids*. 2016;1861(8):793-805. <https://doi.org/10.1016/j.bbalip.2015.12.010>
2. Onal G, Kutlu O, Gozuacik D, Emre SD. Lipid droplets in health and disease. *Lipids Health Dis*. 2017;16(1):128-143. <https://doi.org/10.1186/s12944-017-0521-7>
3. Allwood JW, Winder CL, Dunn WB, Goodacre R. Considerations in sample preparation, collection, and extraction approaches applied in microbial, plant, and mammalian metabolic profiling. In: Lutz NW, Sweedler JV, Wevers RA, eds. *Methodologies for Metabolomics*. New York, NY: Cambridge University Press; 2012. <https://doi.org/10.1017/CBO9780511996634>
4. Kaleigh F, Kurokawa M. Evading apoptosis in cancer. *Trends Cell Biol*. 2013;23(12):620-633. <https://doi.org/10.1038/jid.2014.371>
5. Letai A. Apoptosis and cancer. *Annu Rev Cancer Biol*. 2017;1(1):275-294. <https://doi.org/10.1146/annurev-cancerbio-050216-121933>
6. De Bruin EC, Medema JP. Apoptosis and non-apoptotic deaths in cancer development and treatment response. *Cancer Treat Rev*. 2008;34(8):737-749. <https://doi.org/10.1016/j.ctrv.2008.07.001>
7. Rainaldi G, Romano R, Indovina P, et al. Metabolomics using ^1H NMR of apoptosis and necrosis in HL60 leukemia cells: differences between the two types of cell death and independence from the stimulus of apoptosis used. *Radiat Res*. 2008;169(2):170-180. <https://doi.org/10.1667/RR0958.1>
8. Boren J, Brindle KM. Apoptosis-induced mitochondrial dysfunction causes cytoplasmic lipid droplet formation. *Cell Death Differ*. 2012;19(9):1561-1570. <https://doi.org/10.1038/cdd.2012.34>
9. Milkevitch M, Shim H, Pilatus U, et al. Increases in NMR-visible lipid and glycerophosphocholine during phenylbutyrate-induced apoptosis in human prostate cancer cells. *Biochim Biophys Acta–Mol Cell Biol Lipids*. 2005;1734(1):1-12. <https://doi.org/10.1016/j.bbalip.2005.01.008>
10. Lilimatainen T, Hakumäki JM, Kauppinen RA, Ala-Korpela M. Monitoring of gliomas *in vivo* by diffusion MRI and ^1H MRS during gene therapy-induced apoptosis: Interrelationships between water diffusion and mobile lipids. *NMR Biomed*. 2009;22(3):272-279. <https://doi.org/10.1002/nbm.1320>
11. Adosraku RK, Choi GTY, Constantinou-Kokotos V, Anderson MM, Gibbons WA. NMR lipid profiles of cells, tissues, and body fluids: proton NMR analysis of human erythrocyte lipids. *J Lipid Res*. 1994;35:1925-1931.
12. Bono MS, Garcia RD, Sri-Jayantha DV, Ahner BA, Kirby BJ. Measurement of lipid accumulation in *Chlorella vulgaris* via flow cytometry and liquid-state ^1H NMR spectroscopy for development of an NMR-traceable flow cytometry protocol. *PLoS ONE*. 2015;10(8):e0134846. <https://doi.org/10.1371/journal.pone.0134846>
13. Daemen S, van Zandvoort MAMJ, Parekh SH, Hesselink MKC. Microscopy tools for the investigation of intracellular lipid storage and dynamics. *Mol Metab*. 2016;5(3):153-163. <https://doi.org/10.1016/j.molmet.2015.12.005>
14. Listenberger LL, Studer AM, Brown DA, Wolins NE. Fluorescent detection of lipid droplets and associated proteins. *Curr Protoc Cell Biol*. 2016;71(1):4.31.1-4.31.14. <https://doi.org/10.1002/cpcb.7>
15. Pan X, Wilson M, McConville C, Arvanitis TN, Kauppinen RA, Peet AC. The size of cytoplasmic lipid droplets varies between tumour cell lines of the nervous system: a ^1H NMR spectroscopy study. *Magn Reson Mater Phys Biol Med*. 2012;25(6):479-485. <https://doi.org/10.1007/s10334-012-0315-x>
16. Di Vito M, Lenti L, Knijn A, et al. ^1H NMR-visible mobile lipid domains correlate with cytoplasmic lipid bodies in apoptotic T-lymphoblastoid cells. *Biochim Biophys Acta–Mol Cell Biol Lipids*. 2001;1530(1):47-66. [https://doi.org/10.1016/S1388-1981\(00\)00165-7](https://doi.org/10.1016/S1388-1981(00)00165-7)
17. Pérez Y, Lahrech H, Cabañas ME, et al. Measurement by nuclear magnetic resonance diffusion of the dimensions of the mobile lipid compartment in C6 cells. *Cancer Res*. 2002;62(20):5672-5677.
18. Remy C, Fouilhã N, Barba I, et al. Evidence that mobile lipids detected in rat brain glioma by ^1H nuclear magnetic resonance correspond to lipid droplets. *Cancer Res*. 1997;57:407-4014.
19. Ellis RJ. Macromolecular crowding: obvious but underappreciated. *Trends Biochem Sci*. 2001;26(10):597-604. [https://doi.org/10.1016/S0968-0004\(01\)01938-7](https://doi.org/10.1016/S0968-0004(01)01938-7)
20. Griffin JL, Pole JCM, Nicholson JK, Carmichael PL. Cellular environment of metabolites and a metabolomic study of tamoxifen in endometrial cells using gradient high resolution magic angle spinning ^1H NMR spectroscopy. *Biochim Biophys Acta–Gen Subj*. 2003;1619(2):151-158. [https://doi.org/10.1016/S0304-4165\(02\)00475-0](https://doi.org/10.1016/S0304-4165(02)00475-0)
21. Kono K, Inoue Y, Nakayama K, et al. The role of diffusion-weighted imaging in patients with brain tumors. *Am J Neuroradiol*. 2001;22(6):1081-1088.
22. Wu M, Gmach O, Skurk T, et al. Measuring large lipid droplet sizes by probing restricted lipid diffusion effects with diffusion-weighted MRS at 3T. *Magn Reson Med*. 2019;81(6):1-13. <https://doi.org/10.1002/mrm.27651>
23. Cao P, Fan SJ, Wang AM, et al. Diffusion magnetic resonance monitors intramyocellular lipid droplet size in vivo. *Magn Reson Med*. 2015;73(1):59-69. <https://doi.org/10.1002/mrm.25116>

24. Cheng LL, Ma MJ, Becerra L, et al. Quantitative neuropathology by high resolution magic angle spinning proton magnetic resonance spectroscopy. *Proc Natl Acad Sci U S A*. 1997;94(12):6408-6413. <https://doi.org/10.1073/pnas.94.12.6408>
25. Jagannathan NR, Sharma U. Breast tissue metabolism by magnetic resonance spectroscopy. *Metabolites*. 2017;7(2):25-44. <https://doi.org/10.3390/metabo7020025>
26. Hennebelle M, Roy M, St-Pierre V, et al. Energy restriction does not prevent insulin resistance but does prevent liver steatosis in aging rats on a Western-style diet. *Nutrition*. 2015;31(3):523-530. <https://doi.org/10.1016/j.nut.2014.09.009>
27. Hester S, Griffin JL, Wayland M, et al. Mitochondrial dysfunction in schizophrenia: evidence for compromised brain metabolism and oxidative stress. *Mol Psychiatry*. 2004;9(7):684-697. <https://doi.org/10.1038/sj.mp.4001511>
28. Griffin JL, Blenkiron C, Valonen PK, Caldas C, Kauppinen RA. High-resolution magic angle spinning ^1H NMR spectroscopy and reverse transcription-PCR analysis of apoptosis in a rat glioma. *Anal Chem*. 2006;78(5):1546-1552. <https://doi.org/10.1021/ac051418o>
29. Siminovitch DJ, Ruocco MJ, Olejniczak ET, Das Gupta SK, Griffin RG. Anisotropic ^2H -nuclear magnetic resonance spin-lattice relaxation in cerebroside- and phospholipid-cholesterol bilayer membranes. *Biophys J*. 1988;54(3):373-381. [https://doi.org/10.1016/S0006-3495\(88\)82970-9](https://doi.org/10.1016/S0006-3495(88)82970-9)
30. Fernie AR, Trethewey RN, Krotzky AJ. Metabolite profiling from diagnostics to systems biology. *Nat Rev Mol Cell Biol*. 2004;5(September):763-769.
31. Le Belle JE, Harris NG, Williams SR, Bhakoo KK. A comparison of cell and tissue extraction techniques using high-resolution ^1H NMR spectroscopy. *NMR Biomed*. 2002;15(1):37-44. <https://doi.org/10.1002/nbm.740>
32. Giacomoni F, Le Corguillé G, Monsoor M, et al. Workflow4Metabolomics: a collaborative research infrastructure for computational metabolomics. *Bioinformatics*. 2015;31(9):1493-1495. <https://doi.org/10.1093/bioinformatics/btu813>
33. Griffin JL, Williams HJ, Sang E, Nicholson JK. Abnormal lipid profile of dystrophic cardiac tissue as demonstrated by one and two dimensional magic angle spinning ^1H NMR spectroscopy. *Magn Reson Med*. 2001;46(2):249-255. <https://doi.org/10.1002/mrm.1185>
34. Griffin JL, Bollard M, Nicholson JK, Bhakoo K. Spectral profiles of cultured neuronal and glial cells derived from HRMAS ^1H NMR spectroscopy. *NMR Biomed*. 2002;15(6):375-384. <https://doi.org/10.1002/nbm.792>
35. Wu D, Chen A, Johnson SC. An improved diffusion-ordered spectroscopy experiment incorporating bipolar-gradient pulses. *J Magn Reson A*. 1995; 115(2):260-264. <https://doi.org/10.1006/jmra.1995.1176>
36. Xia J, Sinelnikov IV, Han B, Wishart DS. MetaboAnalyst 3.0—making metabolomics more meaningful. *Nucleic Acids Res*. 2015;43(W1):W251-W257. <https://doi.org/10.1093/nar/gkv380>
37. Tinevez JY, Perry N, Schindelin J, et al. TrackMate: an open and extensible platform for single-particle tracking. *Methods*. 2017;115:80-90. <https://doi.org/10.1016/j.ymeth.2016.09.016>
38. Gibbons E, Pickett KR, Streeter MC, Warcup AO, Judd AM, Bell JD. Molecular details of membrane fluidity changes during apoptosis and relationship to phospholipase A2 activity. *Biochim Biophys Acta*. 2013;1828(2):887-895. <https://doi.org/10.1016/j.bbamem.2012.08.024>
39. Nielson KH, Olsen CA, Allred DV, et al. Susceptibility of S49 lymphoma cell membranes to hydrolysis by secretory phospholipase A(2) during early phase of apoptosis. *Biochim Biophys Acta*. 2000;1484:163-174.
40. Quintero MR, Cabañas ME, Arús C. A possible cellular explanation for the NMR-visible mobile lipid (ML) changes in cultured C6 glioma cells with growth. *Biochim Biophys Acta—Mol Cell Biol Lipids*. 2007;1771(1):31-44. <https://doi.org/10.1016/j.bbalip.2006.10.003>
41. Zietkowski D, Payne GS, Nagy E, Moberley MA, Ryder TA, Desouza NM. Comparison of NMR lipid profiles in mitotic arrest and apoptosis as indicators of paclitaxel resistance in cervical cell lines. *Magn Reson Med*. 2012;68(2):369-377. <https://doi.org/10.1002/mrm.23265>
42. Decorsp M, Lahrech H, Zoula S, Farion R, Remy C. In vivo measurement of the size of lipid droplets in an intracerebral glioma in the rat. *Magn Reson Med*. 2002;45(3):409-414. [https://doi.org/10.1002/1522-2594\(200103\)45:3<409::aid-mrm1053>3.0.co;2-o](https://doi.org/10.1002/1522-2594(200103)45:3<409::aid-mrm1053>3.0.co;2-o)
43. Stejskal EO, Tanner JE. Spin diffusion measurements: spin echoes in the presence of a time-dependent field gradient. *J Chem Phys*. 1965;42(1): 288-292. <https://doi.org/10.1063/1.1695690>
44. Lang I, Scholz M, Peters R. Molecular mobility and nucleocytoplasmic flux in hepatoma cells. *J Cell Biol*. 1986;102(4):1183-1190. <https://doi.org/10.1083/jcb.102.4.1183>
45. Liang L, Xing D, Chen T, Pei Y. Nucleoplasmic viscosity of living cells investigated by fluorescence correlation spectroscopy. *Opt Health Care Biomed Opt III*. 2007;6826(January 2008):6826-2T. <https://doi.org/10.1117/12.760226>
46. García-Pérez AI, López-Beltrán EA, Klüner P, Luque J, Ballesteros P, Cerdán S. Molecular crowding and viscosity as determinants of translational diffusion of metabolites in subcellular organelles. *Arch Biochem Biophys*. 1999;362(2):329-338. <https://doi.org/10.1006/abbi.1998.1051>
47. Ceñido JF, Itin B, Stark RE, et al. Characterization of lipid rafts in human platelets using nuclear magnetic resonance: a pilot study. *Biochem Biophys Rep*. 2017;10(March):132-136. <https://doi.org/10.1016/j.bbrep.2017.03.005>
48. Ye Y, Liu X, Zhang Z, et al. ^{19}F NMR spectroscopy as a probe of cytoplasmic viscosity and weak protein interactions in living cells. *Chemistry*. 2013; 19(38):12705-12710. <https://doi.org/10.1002/chem.201301657>
49. Puchkov EO. Intracellular viscosity: methods of measurement and role in metabolism. *Biochem Suppl A*. 2013;7(4):270-279. <https://doi.org/10.1134/s1990747813050140>
50. Dijksterhuis J, Nijse J, Hoekstra FA, Golovina EA. High viscosity and anisotropy characterize the cytoplasm of fungal dormant stress-resistant spores. *Eukaryot Cell*. 2007;6(2):157-170. <https://doi.org/10.1128/EC.00247-06>
51. Adams DS. Mechanisms of cell shape change: the cytomechanics of cellular response to chemical environment and mechanical loading. *J Cell Biol*. 1992;117(1):83-93. <https://doi.org/10.1083/jcb.117.1.83>
52. Einstein A. On the motion of small particles suspended in a stationary liquid. *Ann Phys (Leipzig)*. 1905;322(8):549-560. <https://doi.org/10.1002/andp.19053220806>
53. Wifflinga F, Haas JT, Walthera TC, Farese RV Jr. Lipid droplet biogenesis. *Curr Opin Cell Biol*. 2014;29:39-45. <https://doi.org/10.1016/j.cbbi.2017.04.008>
54. Martín-Sitjar J, Delgado-Goñi T, Cabañas ME, Tzen J, Arús C. Influence of the spinning rate in the HR-MAS pattern of mobile lipids in C6 glioma cells and in artificial oil bodies. *Magn Reson Mater Phys Biol Med*. 2012;25(6):487-496. <https://doi.org/10.1007/s10334-012-0327-6>
55. Li X, Cox JC, Flumerfelt RW. Determination of emulsion size distribution by NMR restricted diffusion measurement. *AIChE J*. 1992;38(10):1671-1674. <https://doi.org/10.1002/aic.690381019>
56. White NS, McDonald CR, Farid N, et al. Diffusion-weighted imaging in cancer: physical foundations and applications of restriction spectrum imaging. *Cancer Res*. 2014;74(17):4638-4652. <https://doi.org/10.1158/0008-5472.CAN-13-3534>

SUPPORTING INFORMATION

Additional supporting information may be found online in the Supporting Information section at the end of this article.

How to cite this article: Wylot M, Whittaker DTE, Wren SAC, Bothwell JH, Hughes L, Griffin JL. Monitoring apoptosis in intact cells by high-resolution magic angle spinning ^1H NMR spectroscopy. *NMR in Biomedicine*. 2021;34:e4456. <https://doi.org/10.1002/nbm.4456>